Signal reshaping and noise suppression using photonic crystal Fano structures

Bekele, Dagmawi Alemayehu; Yu, Yi; Hu, Hao; Guan, Pengyu; Galili, Michael; Ottaviano, Luisa; Oxenløwe, Leif Katsuo; Yvind, Kresten; Mørk, Jesper

Published in:
Optics Express

Link to article, DOI:
10.1364/OE.26.019596

Publication date:
2018

Document Version
Publisher's PDF, also known as Version of record

Research Article | Vol. 26, No. 15 | 23 Jul 2018 | OPTICS EXPRESS 19596
Optics EXPRESS

Signal reshaping and noise suppression using photonic crystal Fano structures

DAGMAWI A. BEKELE, YI YU, HAO HU, PENGYU GUAN, MICHAEL GALILI, LUISA OTTAVIANO, LEIF KATSUO OXENLØWE, KRESTEN YVIND, AND JESPER MORK*

DTU Fotonik, Department of photonics Engineering, Technical University of Denmark, Dk-2800, Kgs. Lyngby, Denmark
jesm@fotonik.dtu.dk

Abstract: We experimentally demonstrate the use of photonic crystal Fano resonances for reshaping optical data signals. We show that the combination of an asymmetric Fano resonance and carrier-induced nonlinear effects in a nanocavity can be used to realize a nonlinear power transfer function, which is a key functionality for optical signal regeneration, particularly for suppression of amplitude fluctuations of data signals. The experimental results are explained using simulations based on coupled-mode theory and also compared to the case of using conventional Lorentzian-shaped resonances. Using indium phosphide photonic crystal membrane structures, we demonstrate reshaping of 2 Gbit/s and 10 Gbit/s return-to-zero on-off keying (RZ-OOK) data signals at telecom wavelengths around 1550 nm. Eye diagrams of the reshaped signals show that amplitude noise fluctuations can be significantly suppressed. The reshaped signals are quantitatively analyzed using bit-error ratio (BER) measurements, which show up to 2 dB receiver sensitivity improvement at a BER of 10^{-9} compared to a degraded input noisy signal. Due to efficient light-matter interaction in the high-quality factor and small mode-volume photonic crystal nanocavity, low energy consumption, down to 104 fJ/bit and 41 fJ/bit for 2 Gbit/s and 10 Gbit/s, respectively, has been achieved. Device perspectives and limitations are discussed.

OCIS codes: (070.4340) Nonlinear optical signal processing; (200.6015) Signal regeneration; (050.5298) Photonic crystals; (230.1150) All-optical devices.

References and links

1. O. Leclerc, B. Lavigne, E. Balmefrezol, P. Brindel, L. Pierre, D. Rouvillain, and F. Seguineau, "Optical regeneration at 40 Gb/s and beyond," J. Lightwave Technol. **21**, 2779–2790 (2003).
2. G. P. Agrawal, *Fiber-Optic Communication Systems*, 4th ed. (John Wiley & Sons, 2012).
3. A. E. Willner, S. Khaleghi, M. R. Chitgarha, and O. F. Yilmaz, "All-optical signal processing," J. Lightwave Technol. **32**, 660–680 (2014).
4. R. Slavík, F. Parmigiani, J. Kakande, C. Lundström, M. Sjödin, P. A. Andrekson, R. Weerasuriya, S. Sygletos, A. D. Ellis, L. Grüner-Nielsen, D. Jakobsen, S. Herstrøm, R. Phelan, J. O'Gorman, A. Bogris, D. Syvridis, S. Dasgupta, P. Petropoulos, and D. J. Richardson, "All-optical phase and amplitude regenerator for next-generation telecommunications systems," Nat. Photonics **4**, 690–695 (2010).
5. F. Öhman, S. Bischoff, B. Tromborg, and J. Mørk, "Noise and Regeneration in Semiconductor Waveguides With Saturable Gain and Absorption," IEEE J. Quantum Electron. **40**, 245–255 (2004).
6. J. Mørk, F. Öhman, and S. Bischoff, "Analytical expression for the bit error rate of cascaded all-optical regenerators," IEEE Photonics Technol. Lett. **15**, 1479–1481 (2003).
7. K. Lengle, M. Gay, A. Bazin, I. Sagnes, R. Braive, P. Monnier, L. Bramerie, N. Nguyen, C. Pareige, R. Madec, J. C. Simon, R. Raj, and F. Raineri, "Fast All-Optical 10 Gb/s NRZ Wavelength Conversion and Power Limiting Function using Hybrid InP on SOI Nanocavity," Eur. Conf. Exhib. Opt. Commun. We.2.E.5 (2012).
8. T. H. Nguyen, K. Lengle, A. Bazin, L. Bramerie, C. Peucheret, M. Gay, O. Sentieys, J. C. Simon, R. Raj, and F. Raineri, "Phase-preserving power limiting function using InP on SoI photonic crystal nanocavity," IEEE Photonics Technol. Lett. **26**, 1215–1218 (2014).
9. R. Salem, M. A. Foster, A. C. Turner, D. F. Geraghty, M. Lipson, and A. L. Gaeta, "Signal regeneration using low-power four-wave mixing on silicon chip," Nat. Photonics **2**, 35–38 (2008).
10. P. Mechet, T. Spuesens, S. Werquin, K. Vandoorne, N. Olivier, J. M. Fedeli, P. Regreny, D. Van Thourhout, G. Roelkens, and G. Morthier, "All-optical low-power 2R regeneration of 10-Gb/s NRZ signals using a III-V on SOI

#331002 https://doi.org/10.1364/OE.26.019596
Journal © 2018 Received 7 May 2018; revised 10 Jul 2018; accepted 11 Jul 2018; published 19 Jul 2018

Optics EXPRESS

microdisk laser," IEEE Photonics J. **5**, 7802510 (2013).
11. M. Tassaert, H. J. S. Dorren, G. Roelkens, and O. Raz, "Passive InP regenerator integrated on SOI for the support of broadband silicon modulators," Opt. Express **20**, 11383–11388 (2012).
12. T. Vivero, N. Calabretta, I. Tafur Monroy, G. Kassar, F. Öhman, K. Yvind, A. P. González-Marcos, and J. Mørk, "2R-Regeneration in a monolithically integrated four-section SOA-EA chip," Opt. Commun. **282**, 117–121 (2009).
13. Y. Yu, H. Hu, L. K. Oxenløwe, K. Yvind, and J. Mork, "Ultrafast all-optical modulation using a photonic-crystal Fano structure with broken symmetry," Opt. Lett. **40**, 2357 (2015).
14. D. A. Bekele, Y. Yu, H. Hu, P.-Y. Bony, L. Ottaviano, L. K. Oxenløwe, K. Yvind, and J. Mork, "Optical time domain demultiplexing using Fano resonance in InP photonic crystals," in 2017 CLEO/Europe-EQEC) (IEEE, 2017), pp. 1.
15. Y. Yu, W. Xue, E. Semenova, K. Yvind, and J. Mork, "Demonstration of a self-pulsing photonic crystal Fano laser," Nat. Photonics **11**, 81–84 (2017).
16. Y. Yu, Y. Chen, H. Hu, W. Xue, K. Yvind, and J. Mork, "Nonreciprocal transmission in a nonlinear photonic-crystal Fano structure with broken symmetry," Laser Photonics Rev. **9**, 241–247 (2015).
17. D. A. Bekele, Y. Yu, H. Hu, P. Guan, L. Ottaviano, M. Galili, L. K. Oxenløwe, K. Yvind, and J. Mork, "Pulse carving using nanocavity-enhanced nonlinear effects in photonic crystal Fano structures," Opt. Lett. **43**, 955 (2018).
18. S. Fan, "Sharp asymmetric line shapes in side-coupled waveguide-cavity systems," Appl. Phys. Lett. **80**, 908–910 (2002).
19. M. Heuck, P. T. Kristensen, Y. Elesin, and J. Mørk, "Improved switching using Fano resonances in photonic crystal structures," Opt. Lett. **38**, 2466 (2013).
20. A. E. Miroshnichenko, S. Flach, and Y. S. Kivshar, "Fano resonances in nanoscale structures," Rev. Mod. Phys. **82**, 2257–2298 (2010).
21. Y. Shuai, D. Zhao, Z. Tian, J.-H. Seo, D. V. Plant, Z. Ma, S. Fan, and W. Zhou, "Double-layer Fano resonance photonic crystal filters," Opt. Express **21**, 24582 (2013).
22. M. F. Limonov, M. V. Rybin, A. N. Poddubny, and Y. S. Kivshar, "Fano resonances in photonics," Nat. Photonics **11**, 543–554 (2017).
23. Y. Yu, M. Heuck, H. Hu, W. Xue, C. Peucheret, Y. Chen, L. K. Oxenløwe, K. Yvind, and J. Mørk, "Fano resonance control in a photonic crystal structure and its application to ultrafast switching," Appl. Phys. Lett. **105**, 061117 (2014).
24. A. D. Osterkryger, J. R. de Lasson, M. Heuck, Y. Yu, J. Mørk, and N. Gregersen, "Spectral symmetry of Fano resonances in a waveguide coupled to a microcavity," Opt. Lett. **41**, 2065 (2016).
25. Z. Zhang and M. Qiu, "Small-volume waveguide-section high Q microcavities in 2D photonic crystal slabs.," Opt. Express **12**, 3988–3995 (2004).
26. J. D. Joannopoulos, S. G. Johnson, J. N. Winn, and R. D. Meade, *Photonic Crystals: Molding the Flow of Light* (Princeton University, 2011).
27. D. A. Bekele, Y. Yu, H. Hu, Y. Ding, A. Sakanas, L. Ottaviano, E. Semenova, L. K. Oxenløwe, K. Yvind, and J. Mork, "Photonic crystal Fano resonances for realizing optical switches, lasers, and non-reciprocal elements," Proc. SPIE **10345**, 103451V (2017).
28. Yunhong Ding, H. Ou, and C. Peucheret, "Ultra-high-efficiency apodized grating coupler using a fully etched photonic crystal," in *2013 Conference on Lasers and Electro-Optics Pacific Rim (CLEOPR)* (IEEE, 2013), pp. 1–2.
29. W. Suh, Z. Wang, and S. Fan, "Temporal coupled-mode theory and the presence of non-orthogonal modes in lossless multimode cavities," IEEE J. Quantum Electron. **40**, 1511–1518 (2004).
30. Y. Yu, E. Palushani, M. Heuck, N. Kuznetsova, P. T. Kristensen, S. Ek, D. Vukovic, C. Peucheret, L. K. Oxenløwe, S. Combrié, A. de Rossi, K. Yvind, and J. Mørk, "Switching characteristics of an InP photonic crystal nanocavity: experiment and theory," Opt. Express **21**, 31047–61 (2013).
31. K. Nozaki, T. Tanabe, A. Shinya, S. Matsuo, T. Sato, H. Taniyama, and M. Notomi, "Sub-femtojoule all-optical switching using a photonic-crystal nanocavity," Nat. Photonics **4**, 477–483 (2010).
32. A. E. Miroshnichenko and Y. S. Kivshar, "Engineering Fano resonances in discrete arrays," Phys. Rev. E **72**, 056611 (2005).
33. D. A. B. Miller, "Device requirements for optical interconnects to silicon chips," Proc. IEEE **97**, 1166–1185 (2009).
34. M. Heuck, P. T. Kristensen, and J. Mørk, "Energy-bandwidth trade-off in all-optical photonic crystal microcavity switches," Opt. Express **19**, 18410 (2011).
35. B. Lavigne, P. Guerber, P. Brindel, E. Balmefrezol, and B. Dagens, "Cascade of 100 optical 3R regenerators at 40 Gbit/s based on all-active Mach Zehnder interferometers," in *Proc. 27th ECOC* (2001), pp. 290–291.

1. Introduction

Optical signal regeneration is a process that is used to *clean-up* a data signal which has been degraded by noise and other signal impairments [1]. It can be performed either electrically or optically. Electrical signal regeneration involves detecting the incoming optical signal and retransmitting it back into the optical domain [2–4]. Even though electrical regeneration provides very efficient signal regeneration, it consumes significant power due to the use of optoelectronic conversion units, which furthermore limit the operation speed leading to transmission bottlenecks

Optics EXPRESS

[3,4]. On the other hand, optical regeneration offers substantial benefits due to faster processing speed, while avoiding the use of optoelectronic converters [3–5]. Here, we focus on the use of small-footprint and low-energy consumption all-optical devices for signal regeneration, particularly for signal reshaping. The basic principle of signal reshaping is shown in Fig. 1. A noisy data signal having large amplitude fluctuations in the '0' and '1' bit, cf. Fig. 1(b), can be improved by a device having an ideal step-like power transfer function shown in Fig. 1(a). The resulting clean signal is shown in Fig. 1(c) having low amplitude fluctuations and larger extinction ratio (ER) compared to the input noisy signal. In most cases, transfer functions closer to an ideal step functions can be obtained by cascading two or more reshaping stages at the expense of added noise [6]. Each of these stages usually exhibit either of the power transfer functions shown in Fig. 1(d), which are suitable for amplitude fluctuation limiting of '1' bit [region (i)] and '0' bit [region (ii)].

Various experimental studies on signal reshaping using integrated photonics have been reported, such as power limiting of 10 Gbit/s non-return-to-zero (NRZ) signals [7] and phase-preserving 20 Gbit/s NRZ quadrature phase-shift keying signals [8] using Lorentzian resonances based on an indium phosphide/silicon (InP/Si) hybrid photonic crystal (PhC) nanocavity. Reshaping, ER improvement and timing jitter reduction of 10 Gbit/s return-to-zero (RZ) signals have been demonstrated using four-wave mixing in silicon nanowaveguides [9]. Also, ER improvement of a 10 Gbit/s NRZ signal using microdisk lasers integrated on silicon [10], ER improvement up to 2 dB for 1 Gbit/s NRZ signal using a membrane InP switch [11], and reshaping and reamplification of 10 Gbit/s NRZ signals using a semiconductor optical amplifier cascaded with a saturable absorber [12] have been demonstrated.

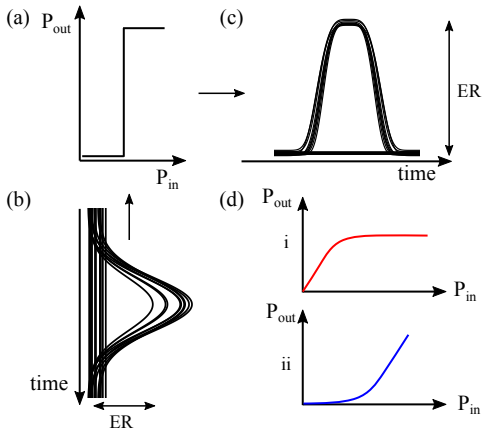

Fig. 1. Basic principle of signal reshaping. (a) Step-like power transfer function of an ideal signal reshaping device. (b) A noisy input optical data signal with small extinction ratio (ER) and large power fluctuations in the '0' and '1' bit levels. (c) Reshaped data signal using the transfer function in part (a) resulting in a clean signal with large ER. (d) Commonly implemented power transfer functions for suppressing power fluctuations in '1' bit (i) and '0' bit (ii). P_{in} and P_{out} denote input and output powers, respectively.

In this paper, we demonstrate the use of sharp asymmetric lineshapes known as Fano resonances for all-optical reshaping of RZ data signals. These Fano resonances accompanied by carrier-induced nonlinear effects are the key enabling features of our devices. We have experimentally realized two types of Fano resonance lineshapes whose nonlinear power transfer functions are suitable for suppressing amplitude fluctuations of '0' and '1' bit of optical data signals. The noise suppression performance of the devices is analyzed in system experiments using eye diagrams and bit-error ratio (BER) tests with data rates up to 10 Gbit/s. Using similar PhC

Optics EXPRESS

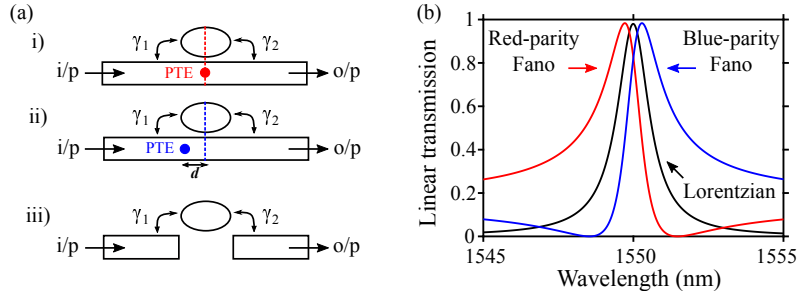

Fig. 2. Lorentzian and Fano resonance structures and corresponding lineshapes. (a) Schematic of structures for realizing red-parity Fano (i), blue-parity Fano (ii), and Lorentzian (iii) resonances. (b) Red and blue-parity Fano resonances compared with Lorentzian resonance lineshape. All resonances have the same total quality factor of 1200 and resonance wavelength of 1550 nm. The amplitude transmission coefficient of the partially-transmitting element (PTE) is 0.4 for red as well as blue-parity Fano resonances.

Fano structures, we have previously demonstrated wavelength conversion [13], optical time domain demultiplexing [14], continuous wave and pulsed mode lasing [15], non-reciprocal transmission [16], and pulse carving [17] applications. Here, we have added a new class of applications of Fano resonances for optical signal reshaping.

2. Photonic crystal Fano structures

A Fano resonance occurs due to the interference between two paths, one of which has a continuum character, while the other involves a discrete resonance, leading to characteristic lineshapes [18–20]. In particular, asymmetric lineshapes imply the appearance of a transmission maximum and a transmission minimum that are closely spaced spectrally, with prospects for linear and nonlinear filtering applications [21, 22]. The structures we investigate involve a nanocavity that is side-coupled to a line-defect waveguide. Figure 2(a) shows schematic diagrams of coupled waveguide-cavity structures for realization of Fano and Lorentzian resonances. For Fano structures, shown in Fig. 2(a) regions (i) and (ii), there is a direct path to the output port mainly determined by the transmission coefficient of the partially transmitting element (PTE) placed in the middle of the waveguide [13, 19, 23]. In contrast, for the Lorentzian structure, shown in Fig. 2(a) region (iii), coupling to the output port is only possible through the cavity. By controlling the size and location of the PTE, both the parity and the shape of the Fano resonance spectrum can be engineered [23, 24]. The parity of a Fano resonance expresses whether the transmission minimum is red-shifted (red-parity) or blue-shifted (blue-parity) compared to the transmission maximum [24], cf. Fig. 2(b). In some literature [20], the blue (red) parity Fano resonances are denoted using positive (negative) values of the asymmetry parameter of the Fano lineshape. Depending on the distance between the cavity center and the PTE, a Fabry-Perot (FP) cavity of length (d) can be formed. The round-trip phase of this FP cavity at the transmission minimum determines the parity of the Fano resonance spectrum as analyzed theoretically in [24]. Furthermore, the spectral separation between the transmission minimum and maximum for the symmetric case ($d = 0$) can be written as $\Delta\omega = \gamma/t_B r_B$, where γ is the total cavity field decay rate into the input and output ports given by $\gamma = \gamma_1 + \gamma_2$ and $\gamma_1 = \gamma_2$. The constants t_B and r_B are the field amplitude transmission and reflection coefficients of the PTE, respectively, which are related by $t_B^2 + r_B^2 = 1$. For simplicity of our calculation, the out-of-plane decay rate from the cavity is neglected, which is a good approximation when the nanocavity is strongly coupled to the waveguide. The minimum extrema separation is then calculated to be $(\Delta\omega)_{min} = 2\gamma$ and it can be achieved when $t_B = 1/\sqrt{2}$. Therefore, the smallest spectral separation between the

Optics EXPRESS

transmission maximum and minimum of an asymmetric Fano resonance is equal to the linewidth of a Lorentzian resonance (2γ).

Our platform for the realization of Fano resonances is an InP photonic crystal (PhC) membrane structure, composed of hexagonally arranged airholes, as shown using the scanning electron microscope (SEM) images in Figs. 3(a) and 3(c). The PhC device is composed of airholes with a radius of ~125 nm and a lattice constant (a) of ~447 nm. The line-defect waveguide is a $W1$-defect formed by removing a single row of airholes and shifting the innermost airholes towards the waveguide center [13], while the nanocavity is of the $H0$ type formed by shifting the airholes around the nanocavity away from the cavity center [25]. The waveguide supports a continuum of guided modes, while the nanocavity only supports a few discrete cavity modes [26]. The interference between these two optical paths creates an asymmetric Fano resonance lineshapes shown in Figs. 3(b) and 3(d). For the device in Fig. 3(a), the PTE airhole is placed in the midplane passing through the center of the cavity ($d = 0$) while for the device in Fig. 3(c) the PTE airhole is placed one lattice constant to the left of the midplane ($d = a$). In both cases, the PTE airhole has a radius of ~123 nm.

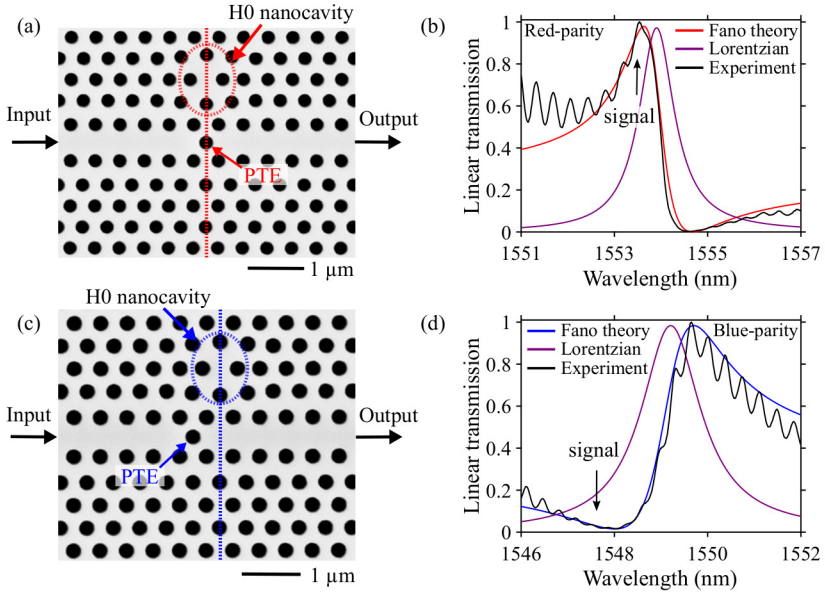

Fig. 3. Photonic crystal (PhC) Fano structures and resonance lineshapes. (a) Scanning electron microscope (SEM) image of the fabricated PhC with the PTE placed at the mid-plane passing through the cavity center. (b) Measured (black line) and simulated (red) transmission spectrum of the device in part (a) showing a red-parity Fano resonance. It is compared to the transmission of a Lorentzian (purple) resonance having the same Q-factor and resonance wavelength as the red-parity Fano resonance. (c) SEM of the device with the PTE placed one lattice constant to the left from the mid-plane. (d) Measured (black) and simulated (blue) transmission spectrum of the device in part (c) exhibiting a blue parity Fano resonance. It is compared with Lorentzian (purple) transmission having the same Q-factor and resonance wavelength as the blue-parity Fano resonance.

The PhC structure is patterned using electron beam lithography with a silicon nitride hard mask, the pattern is then transferred to the InP device layer using a reactive ion etching process. Finally, selective membranization of the PhC is achieved using a wet etching process. The thickness of the PhC membrane is ~340 nm. Grating couplers are used to couple light into and out of the device [27, 28], giving a fiber-to-chip coupling loss of ~10 dB. More details about the device

Optics EXPRESS

structure and fabrication can be found in [27].

The total quality (Q) factors of the nanocavities, estimated using coupled-mode theory (CMT) [29] fits to the measurements in Figs. 3(b) and 3(d), are $Q \approx 1700$ and $Q \approx 1000$ for the red and blue-parity Fano resonances respectively. The intrinsic Q-factor of the nanocavities calculated using 3D finite-difference time domain simulation is $\sim 1.2\times10^5$. The field amplitude transmission coefficient t_B is estimated to be 0.55 and 0.5 for blue and red-parity Fano resonances respectively. Furthermore, the ratio of the decay rates γ_1/γ_2 estimated using CMT fits are 1 and 1.5 for the red and blue-parity Fano resonances respectively. Other parameters used in the simulation are similar to the work reported in [30].

3. Nonlinear power transfer function of Fano resonances

Another key feature of our InP photonic crystal platform is the ability to induce a resonance shift using carrier-induced nonlinear effects. Due to the strongly localized nature of the nanocavity mode, a large number of free-carriers are generated inside the nanocavity via two-photon absorption (TPA) of the optical input signal [31]. This TPA followed by free-carrier dispersion results in a reduction of the refractive index and hence a resonance blue-shift [30]. Similar tuning of Fano resonances using optical Kerr nonlinearities have been theoretically investigated in [32]. Figure 4 presents the nonlinear power transfer functions of the two-types of Fano resonances compared with the case of using Lorentzian resonances. The signal is spectrally centered at the transmission maximum of the red-parity Fano resonance (1553.6 nm), and at the transmission minimum of the blue-parity Fano resonance (1547.5 nm), as indicated by the arrows in Figs. 3(b) and 3(d). Furthermore, the red (blue) parity Fano resonance is compared to the Lorentzian resonance, shown in 3(b) and (d), for which the input signal is placed around its peak (minimum) transmission i.e. 1553.9 nm (1547.5 nm).

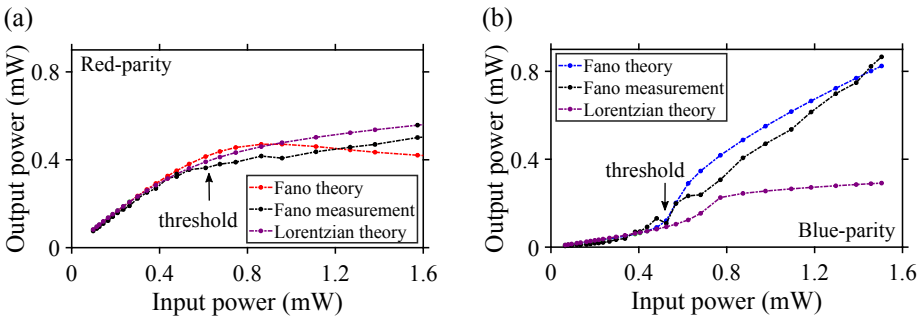

Fig. 4. Nonlinear power transfer functions of red and blue-parity Fano resonances compared with Lorentzian resonance. (a) Measured (black line) and CMT simulated (red line) power transfer function of red-parity Fano resonance compared with simulated Lorentzian (purple line) transfer function. Here, the spectral locations of the input signals are at 1553.6 nm and 1556.9 nm for red-parity Fano and Lorentzian resonances, respectively. (b) Measured (black line) and simulated (blue line) power transfer function of blue-parity Fano resonance compared with simulated Lorentzian (purple line) transfer function. The spectral location of the input signal is at 1547.5 nm for both blue-parity and Lorentzian resonances.

The red-parity Fano resonance exhibits measured (black line) and calculated (red line) nonlinear power transfer functions as shown in Fig. 4(a). The input signal is a train of ~10 ps pulses with a repetition rate of 10 GHz. Initially, the output power follows the linear increase of the input power. However, as the input power increases above 0.5 mW, the output power saturates. This is because of the induced blueshift of the Fano resonance which results in a transmission decrease at the signal spectral position. Therefore, higher input powers are counterbalanced by

Optics EXPRESS

an equivalent reduction in transmission leading to saturation. The deviation of the measured transfer function from that of the CMT simulations may be caused by thermal effects which counterbalance the blue resonance shift. However, the comparison to the theoretical result for a Lorentzian resonance predicts that the red-parity Fano resonance has better power saturation due to the steeper transmission lineshape. Note that the arrows in Figs. 4(a) and 4(b) show the threshold operation points. These points are adjustable by proper choice of the signal spectral detuning compared to the resonance wavelengths, which determines the fraction of the input power coupling to the nanocavity.

Measured (black line) and calculated (blue line) nonlinear power transfer functions for the blue-parity Fano resonances are presented in Fig. 4(b). The input signal is a train of ~30 ps pulses with a repetition rate of 1 GHz. At low input powers, the transmission through the device is very low since the signal is located around the transmission minimum. However, when the average input power increases beyond 0.5 mW, the resonance starts to blueshift which leads to increased transmission of the signal. This results in saturable absorber-like transmission characteristics. On the other hand, the signal transmission for the Lorentzian resonance starts to saturate for increasing resonance shifts and does not exhibit saturable absorber-like transmission.

Therefore, the device exhibiting a red-parity Fano resonance displays nonlinear saturation of the power transmission, while the blue-parity device is suitable for applications requiring saturable absorber-like transmission, cf. Fig. 1(d). These functionalities could help to limit amplitude fluctuations of the '1' and '0' bit of optical data signals.

4. Signal reshaping experiments

In this section, we present experimental investigations of the application of the red-parity Fano resonance for signal reshaping of optical data signals, suppressing amplitude fluctuations of the '1' bit and generating a better-quality signal.

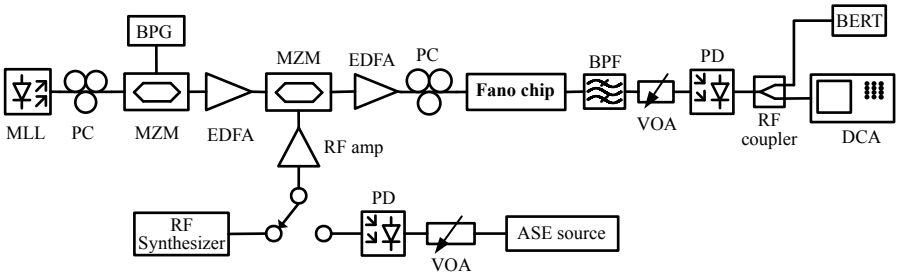

Fig. 5. Measurement setup for signal reshaping experiments. Light from a mode-locked laser (MLL) is on-off keying (OOK) modulated at 2 Gbit/s and 10 Gbit/s in a Mach-Zehnder modulator (MZM) driven by a PRBS of $2^{15} - 1$ generated by a bit-pattern generator (BPG). Intensity fluctuations either from an RF synthesizer or from a random noise source are added to the RZ-OOK signal using a second MZM. This degraded input signal is then fed to the Fano device and the reshaped signal is analyzed at the receiver using bit-error ratio test (BERT) and the eye diagrams are measured using a digital communication analyzer (DCA).

Our signal reshaping experimental setup is shown in Fig. 5. Light from a mode-locked laser (MLL) is polarization controlled (PC) and on-off keying (OOK) modulated at 2 Gbit/s or 10 Gbit/s in a Mach-Zehnder modulator (MZM) driven by pseudo-random bit-sequence length of $2^{15} - 1$ generated by a bit-pattern generator (BPG). Two implementations of intensity noise were introduced on the optical signal. The first employs a signal generated by a radio frequency (RF) synthesizer operated at 500 MHz while the second is a random noise source, implemented using an amplified spontaneous emission (ASE) source, whose output power is controlled by a variable optical attenuator (VOA) before launching into a photodiode (PD). The RF signal from either

Optics EXPRESS

source is used to drive a second MZM, which imposes these intensity fluctuations on top of the reference *clean* RZ-OOK signal to emulate a degraded input signal. The resulting signal is amplified using an erbium-doped fiber-amplifier (EDFA) and coupled into the photonic crystal red-parity Fano chip, which suppresses amplitude fluctuations giving rise to a cleaned signal. This reshaped signal is then compared to the reference and degraded input signals at the receiver by measuring eye diagrams using a digital communication analyzer (DCA) oscilloscope, and bit error ratio using a bit-error ratio tester (BERT). Reference and degraded signals are measured after passing through an on-chip reference waveguide.

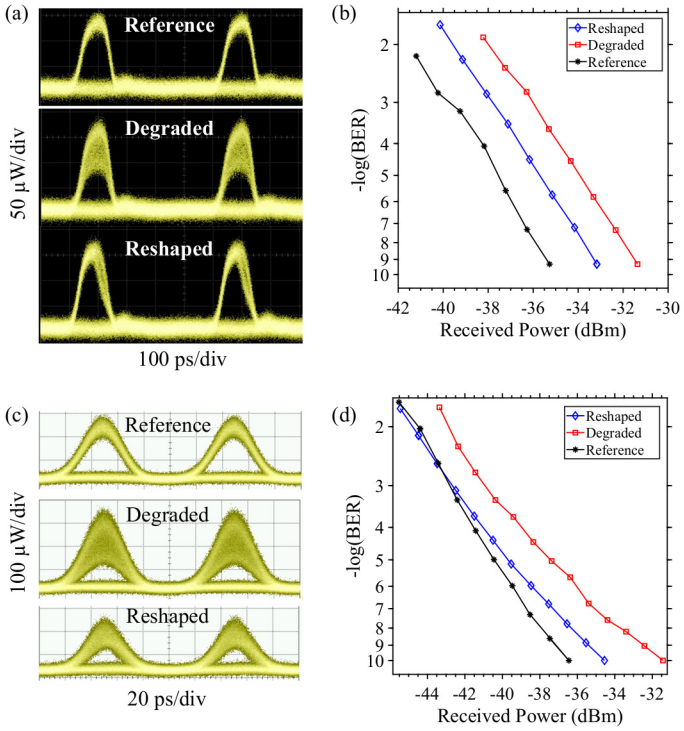

Fig. 6. Noise suppression of RZ-OOK signals using red-parity Fano resonance. (a) and (c) show RZ-OOK eye diagrams of 2 Gbit/s and 10 Gbit/s modulated reference signals without noise (top), the input degraded signal with 500 MHz intensity noise (middle) and the reshaped signal (bottom) respectively. The BER performance measurements for 2 Gbit/s and 10 Gbit/s are shown in (b) and (d) respectively.

Results for the signal reshaping measurements are presented in Fig. 6. Here, we have investigated the noise suppression performance of the device towards intensity noise generated by a 500 MHz sinusoidal signal. The frequency of the sinusoidal signal is selected so that amplitude fluctuations are slower than the modulation speeds of the data signals, which are at 2 Gbit/s and 10 Gbit/s. Figure 6(a) shows eye diagrams for a 2 Gbit/s modulated reference signal (top), degraded signal (middle) and the reshaped signal (bottom). It can be inferred that the amplitude fluctuations in the '1' bit level are reduced, improving the eye opening of the reshaped signal. To quantify this, measured BER as function of received power are shown in Fig. 6(b). The reshaped signal shows a 2 dB receiver sensitivity improvement compared to the degraded signal at a BER of 10^{-9}. Similarly, the measurements are performed for a 10 Gbit/s RZ-OOK signal. The eye diagrams for the reference, degraded and reshaped are shown in Fig. 6(c). Additionally, Fig. 6(d) shows that

Optics EXPRESS

the reshaped signal (blue) has a 2 dB receiver sensitivity improvement at a BER of 10^{-9}. The energy consumption of the devices for these noise suppression experiments are estimated to be 104 fJ/bit and 41 fJ/bit for 2 Gbit/s and 10 Gbit/s, respectively.

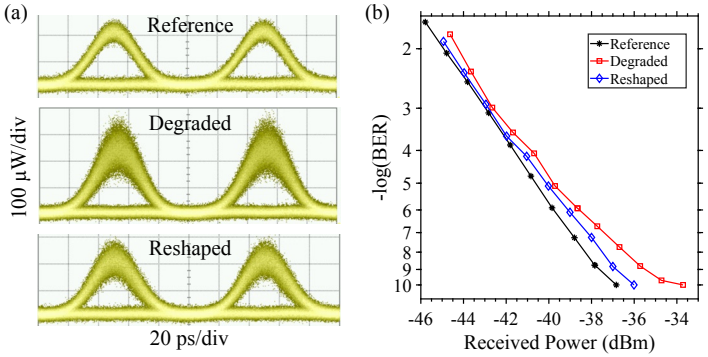

Fig. 7. Suppression of random intensity noise. (a) Eye diagrams of 10 Gbit/s RZ -OOK for the reference (top), degraded with random noise (middle) and reshaped (bottom) signals. (b) The BER measurements for signals shown in part (a).

Intensity fluctuation of data signals in real systems, however, do not have a fixed frequency as investigated in the experiments above. Therefore, we used the random noise source, cf. Fig. 5, which has a bandwidth twice as large as the highest data modulation speed. Figure 7(a) shows the eye diagrams for the reference signal (top), degraded signal with random noise (middle) and reshaped signal (bottom). The BER performance measurements are shown in Fig. 7(b). The reshaped signal (blue) shows a 1 dB receiver sensitivity improvement at a BER of 10^{-9} compared to the degraded signal (red) with an energy consumption down to 47 fJ/bit.

5. Discussion

In this section, we discuss the device limitations, choice of input signal bandwidth, and the prospects of further improving the device performance for signal reshaping applications. For these experiments, operations at data rates higher than 10 Gbit/s was not achieved. This limitation is due to the slow recovery of the device, which is estimated to be around 12 ps [14]. Furthermore, our red-parity Fano resonance device fails to suppress noise fluctuations of signals with average power levels beyond the level at which the resonance shifts past the minimum of the transmission. This is because high input powers will introduce pulse carving effect which distorts the pulse shape [17]. Due to this, the Fano resonance structure cannot be employed to power-limit NRZ modulated signals, which have higher average power than that of RZ signals [33]. On the other hand, from the CMT based calculations, the Lorentzian resonance shows less pulse distortion effect even at higher input power levels since larger resonance shifts are always accompanied by lower signal transmission due to the monotonous decrease of the transmission off the resonance peak. So the Lorentzian structure is particularly advantageous for noise suppression of NRZ signals, as demonstrated in [7, 8].

The limitation of our blue-parity Fano resonance is that the spectral overlap between the cavity resonance and the input signal, which is placed spectrally blue detuned from the minimum of the Fano resonance, is small. This reduces the fraction of the input power coupling to the nanocavity leading to an inefficient nonlinear process. This could be improved by designing the cavity resonance frequency to be closer to the transmission minimum of the Fano resonance. One can achieve this by optimizing the transmission coefficient of the PTE and the Q-factor of the nanocavity, hence enhancing the power coupling into the nanocavity.

Optics EXPRESS

The choice of input signal bandwidth depends on several factors. For the present device, the red-parity Fano resonance has a total Q-factor around 1700, corresponding to a photon life time of $\sim$ 1.4 ps and a cavity linewidth of $\sim$ 0.9 nm, assuming Lorentzian lineshape. Considering a blue-shift of the resonance corresponding to a full swing from transmission maximum to minimum spectral location, the input signal must have a bandwidth that is smaller than the Fano extrema separation, i.e. 1 nm. This ensures that the transmission of the input signal is strongly modulated because of the nonlinear resonance shift [34]. Assuming Gaussian pulses, we have found that the shortest input pulse should be $\sim$ 5 ps [17]. For our experiments, we have used mode a locked laser source generating $\sim$ 10 ps pulses corresponding to signal bandwidth of $\sim$ 0.35 nm. For a given signal bandwidth, the Fano device is optimized, with the coupling to the waveguide and the radius of the airhole being the primary design parameters.

The reshaping experiments presented in this work are simplified proof-of-concept demonstrations of the device performance. In real reshaping and regeneration experiments, cascaded fiber transmission links, e.g. via the use of a re-circulating loop, should be implemented in which case the properties of fiber links such as dispersion and propagation losses have to be taken into account, truly demonstrating the regeneration property of the device for minimizing noise accumulation [35].

6. Conclusion

We have demonstrated all-optical signal reshaping applications using InP photonic crystal Fano resonance structures. By combining two types of sharp asymmetric Fano resonance lineshapes with efficient carrier-induced nonlinear effects in the nanocavity, nonlinear power transfer functions have been measured and validated. Using these nonlinear transfer functions, we proposed the use of red-parity and blue-parity Fano resonances for suppressing noise fluctuations of the '1' and '0' bit levels of optical data signals, respectively. The noise suppression functionality of the red-parity Fano resonance is demonstrated for RZ-OOK modulated signals up to 10 Gbit/s with low energy consumption down to 41 fJ/bit. Additionally, we have shown that the use of blue-parity Fano resonances is effective for the realization of a saturable absorber-like threshold.

Funding

Financial support from Villum Fonden via the NAnophotonics for TErabit Communications (NATEC) center of excellence under grant number 8692 is gratefully acknowledged.